HHS Public Access

Author manuscript

Biomaterials. Author manuscript; available in PMC 2016 July 01.

Published in final edited form as:

Biomaterials. 2015 July ; 57: 41–49. doi:10.1016/j.biomaterials.2015.04.013.

Single Agent Nanoparticle for Radiotherapy and Radio-Photothermal Therapy in Anaplastic Thyroid Cancer

Min Zhou[a,1], **Yunyun Chen**[b,1], **Makoto Adachi**[b], **Xiaoxia Wen**[a], **Bill Erwin**[c], **Osama Mawlawi**[c], **Stephen Y. Lai**[b,*], and **Chun Li**[a,*]

[a]Department of Cancer Systems Imaging, The University of Texas MD Anderson Cancer Center, Houston, Texas 77030 U.S.A

[b]Department of Head and Neck Surgery, and Department of Molecular and Cellular Oncology, The University of Texas MD Anderson Cancer Center, Houston, Texas 77030 U.S.A

[c]Department of Imaging Physics, The University of Texas MD Anderson Cancer Center, Houston, Texas 77030 U.S.A

Abstract

Anaplastic thyroid carcinoma (ATC) is one of the most aggressive human malignancies. The aggressive behavior of ATC and its resistance to traditional treatment limit the efficacy of radiotherapy, chemotherapy, and surgery. The purpose of this study is aimed at enhancing the therapeutic efficacy of radiotherapy (RT) combined with photothermal therapy (PTT) in murine orthotopic model of ATC, based on our developed single radioactive copper sulfide (CuS) nanoparticle platform. We prepare a new dual-modality therapy for ATC consisting of a single-compartment nanoplatform, polyethylene glycol-coated [^{64}Cu]CuS NPs, in which the radiotherapeutic property of ^{64}Cu is combined with the plasmonic properties of CuS NPs. Mice with Hth83 ATC were treated with PEG[^{64}Cu]CuS NPs and/or near infrared laser. Antitumor effects were assessed by tumor growth and animal survival. We found that in mice bearing orthotopic human Hth83 ATC tumors, micro-PET/CT imaging and biodistribution studies showed that about 50% of the injected dose of PEG-[^{64}Cu]CuS NPs was retained in tumor 48 h after intratumoral injection. Human absorbed doses were calculated from biodistribution data. In antitumor experiments, tumor growth was delayed by PEG-[^{64}Cu]CuS NP-mediated RT, PTT, and combined RT/PTT, with combined RT/PTT being most effective. In addition, combined RT/PTT significantly prolonged the survival of Hth83 tumor-bearing mice compared to no treatment, laser treatment alone, or NP treatment alone without producing acute toxic effects. These findings

Corresponding Author: Chun Li, Department of Cancer Systems Imaging, Unit 1907, The University of Texas MD Anderson Cancer Center, Houston, Texas 77030. Phone: 713-792-5182; Fax: 713-794-5456; cli@mdanderson.org. Stephen Y. Lai*, Department of Head and Neck Surgery, Unit 1445, The University of Texas MD Anderson Cancer Center, Houston, Texas 77030. Phone: 713-792-6528; Fax: 713-794-4662; sylai@mdanderson.org.

[1]these authors contributed equally.

Supplementary data: details on method used for radiolabeling efficiency and hydrodynamic diameter data.

indicate that this single-compartment multifunctional NPs platform merits further development as a novel therapeutic agent for ATC.

Keywords

radiotherapy; dosimetry; positron emission tomography; photothermal ablation therapy; copper-64; anaplastic thyroid cancer

1. Introduction

Approximately 60,220 new cases of thyroid cancer are diagnosed in the United States each year, and the incidence of thyroid malignancies is increasing [1–3]. Anaplastic thyroid cancer (ATC) has perhaps the worst prognosis of any cancer because of its aggressive behavior and resistance to treatment. Although thyroid cancer in general is an uncommon cause of mortality, patients with ATC have a grave prognosis: the mortality rate is almost 100%, and median survival time is about 5 months, with only 20% of patients surviving 1 year after diagnosis [4, 5].

Radiotherapy (RT) is common employed in the treatment of ATC either as definitive treatment or following surgical resection [6]. Patients often die due to locoreginal disease that causes festering non-healing wounds, carotid artery blowouts and suffocation. Multimodality therapy combining RT with other treatment modalities, such as chemotherapy, can prevent death from local invasion and airway compromise [7]. Thus, locoregional control is critical and can improve survival and also quality of life for some patients. Because of the aggressive nature and rarity of ATC, studies of this disease tend to be characterized by small cohorts and short follow-up times, which make it difficult to compare outcomes for different treatments [8, 9]. Novel therapies with different mechanisms of action are likely necessary to achieve any significant improvements over the current depressing outcomes.

Near-infrared (NIR) laser-induced photothermal therapy (PTT), a minimally invasive therapy, has gained increasing attention owing to the favorable biosafety characteristics of NIR light in tissues and a mode of cell death different from that produced by conventional chemotherapy and RT [10]. Nanoparticles (NPs) that absorb light in the NIR region (wavelength, 700–1100 nm) offer an opportunity to convert optical energy into thermal energy, enabling the deposition of otherwise benign optical energy into tumors for thermal ablation of tumor cells. Although noble metal nanostructures are the most widely described photothermal conversion agents for PTT [11–13], semiconductor copper sulfide (CuS) NPs are also attractive photothermal conversion agents because their size can be controlled at around 10 nm while their absorption peak can be readily tuned to 930 to 1100 nm, which makes these NPs suitable for PTT and photoacoustic imaging using a 980-nm laser or a 1064-nm laser [14–16]. For NP-mediated PTT, the use of 980-nm laser has some advantages over the use of 808-nm laser, such as high heat conversion efficiency and availability of laser for clinical use.

A number of radiometal beta-emitting NPs have been suggested as possible agents for cancer RT. An advantage of RT with widely-used β^- particle emitter radionuclides is that the radioactivity can cause substantial damage to the target cancer cells but is unlikely to harm nontarget tissues because the mean range in tissue is less than a few millimeters. NPs labeled with rhenium 186/rhenium 188, yttrium 90, and gold 198 have been tested in preclinical tumor models [17–19]. Copper 64 (^{64}Cu) has also been suggested for RT because it has an intermediate half-life ($T_{1/2}$ = 12.7 h) and decays through β^+ emission (0.655 meV, 19%), β^- emission (0.573 meV, 40%), and electron capture (41%). These radioactivities of ^{64}Cu make it a suitable radioisotope for positron emission tomography (PET) imaging, RT for cancer with β^- particles and Auger electrons, and accurate dosimetry [20–24]. However, no data have been reported to date from *in vitro* or *in vivo* studies of ^{64}Cu-labeled NPs for RT [25].

We recently reported that chelator-free polyethylene glycol (PEG)-coated [^{64}Cu]CuS NPs (PEG-[^{64}Cu]CuS NPs) with strong NIR absorbance can be used for PET image-guided PTT [14]. We now report the use of PEG-[^{64}Cu]CuS NPs for RT and combined radio-photothermal therapy (RT/PTT) in an ATC orthotopic xenograft model. To the best of our knowledge, this is the first report of the tumor-killing effects of ^{64}Cu-labeled NPs for RT and combined RT/PTT mediated by a single-compartment NP platform.

2. Materials and Methods

2.1 Materials

Copper(II) chloride ($CuCl_2$), sodium sulfide ($Na_2S{\cdot}9H_2O$), and methoxy-PEG-thiol (SH-PEG; molecular weight 5000 Da) were purchased from Sigma-Aldrich (St. Louis, MO). Isoflurane was obtained from Baxter (Deerfield, IL). $^{64}CuCl_2$ was obtained from the University of Wisconsin (Madison, WI). All of the chemicals and solvents were at least American Chemical Society grade and were used without further purification. Deionized water (18 MΩ) was obtained from a Milli-Q synthesis system (Millipore, Billerica, MA).

2.2 Synthesis and characterization of PEG-CuS NPs

The nonradioactive analogues, PEG-CuS NPs, were synthesized according to previously reported procedures [14]. Briefly, 40 μL of aqueous solution of sodium sulfide (Na_2S, 1M) was added into a 10-mL aqueous solution of $CuCl_2$ (4 mM) and PEG-SH (1.0 mg) under stirring at room temperature. The reaction mixture was heated to 90°C and stirred for 15 min until a dark green solution was obtained. The mixture was transferred to ice-cold water. The resulting PEG-CuS NPs were purified by ultracentrifugation using an Amicon Ultra-15 Centrifugal Filter Unit (Millipore) and stored at 4°C under nitrogen.

For transmission electron microscopy (TEM), an aqueous solution of CuS NPs was deposited on carbon-enhanced copper grids without negative staining. The NPs were allowed to adhere to the grid for 1 h, after which they were briefly rinsed with deionized water and air-dried. The samples were then examined using a TEM microscope (JEM 2010, JEOL, Japan) at an accelerating voltage of 200 kV. Digital images were obtained using an AMT imaging system (Advanced Microscopy Techniques Corp., Danvers, MA). The ultraviolet-visible spectra of CuS NPs were recorded on a Beckman Coulter DU-800 UV–

Vis spectrometer (Brea, CA) with a 1.0-cm optical-path-length quartz cuvette. Particle size was measured using dynamic light scattering at a 90° scatter angle on a ZetaPLUS particle electrophoresis system (Brookhaven Instruments Corp., Holtsville, NY).

2.3 Synthesis and characterization of PEG-[^{64}Cu]CuS NPs

PEG-[^{64}Cu]CuS NPs were synthesized as described in the preceding section with $^{64}CuCl_2$ in addition to $CuCl_2$. Briefly, $^{64}CuCl_2$ (10 μL, 148 MBq) was added to 190 μL of $CuCl_2$ solution (4 mM) containing PEG-SH (0.2 g/L), after which 8 μL of sodium sulfide solution (100 mM) was added to the $CuCl_2$ solution with stirring. The mixture was then heated to 90°C for 15 min until a dark-green soluti on was obtained. The reaction mixture was transferred to ice-cold water to yield PEG-[^{64}Cu]CuS NPs.

The radiolabeling efficiency and stability of the labeled NPs were analyzed using instant thin-layer chromatography. The chromatography strips were developed with phosphate-buffered saline (pH 7.4) containing 4-mM ethylenediaminetetraacetic acid, and radioactivity was quantified using an IAR-2000 TLC imaging scanner (Bioscan, Washington, DC). To study the labeling stability, PEG-[^{64}Cu]CuS NPs were suspended in phosphate-buffered saline or mouse serum and incubated at 37°C for 24 h. Free $^{64}Cu^{2+}$ ions moved to the solvent front, and the NPs remained at the original spot. The radioactivity at the original spot was recorded as a percentage of the total radioactivity of the chromatography strip.

2.4 Photothermal effect in aqueous solution

The NIR laser system used in this study consists of a commercially available 980-nm diode laser (PhoTex15; Visualase, Inc., Houston, TX). A 5-m-long, 600-μm-core BioTex LCM-001 optical fiber (Houston, TX) was used to transfer laser power from the laser unit to the target. This fiber had a lens mounted at the output that allowed the laser spot size to be changed by changing the distance from the output to the target. The end of the optical fiber was attached to a retort stand using a movable clamp and positioned directly above the tumor. For measurement of temperature change mediated by CuS NPs, NIR laser light (2.5 W/cm^2, spot diameter 10 mm) was delivered through a quartz cuvette containing the CuS NPs (200 μL). A thermocouple was inserted into the aqueous solution of NPs perpendicular to the path of the laser light. The temperature was measured over 10 min. Water was used as a control. Thermographic pictures were taken using a thermal camera (Flir i7, Flir Systems, Inc., Portland, OR).

2.5 Animals and tumor model

All animal handling procedures were in accordance with the guidelines of the Institutional Animal Care and Use Committee of The University of Texas MD Anderson Cancer Center (Houston, TX) and were performed under a protocol approved by this committee. Animal facilities were approved by the American Association for Accreditation of Laboratory Animal Care in accordance with current regulations and standards of the US Department of Agriculture, US Department of Health and Human Services. Male athymic nude mice, age 8 to 12 weeks, weight 25 to 30 g, were purchased from NCI-Frederick Cancer Research and Development Center (Frederick, MD). The mice were fed irradiated mouse chow and housed in laminar flow cabinets under specific pathogen-free conditions.

Hth83 cells were obtained from Dr. Jeffrey N. Myers (UTMDACC, USA), who obtained this cell line from Dr. Nils-Erik Heldin (University of Uppsala, Sweden) [26]. The cell line has been authenticated using short tandem repeat (STR) profiles and identified to be a unique ATC cell line. They were authenticated again in August, 2012. To obtain an orthotopic nude mouse model of ATC, Hth83-lucif cells (5×10^5 cells/mouse) were injected orthotopically into the right thyroid gland of male athymic nude mice as previously described [8]. The tumors were allowed to grow for 10 to 12 days, until tumor size reached 30 to 50 mm^3, and then the mice were imaged using an IVIS 200 bioluminescence imaging system (Xenogen Corp., Waltham, MA) to monitor tumor burden.

2.6 Bioluminescence imaging of orthotopic thyroid tumors

The mice with Hth83-lucif tumors were anesthetized using 2% isoflurane (Abbott, Abbott Park, IL). An aqueous solution of D-Luciferin (1 mg/mL; Xenogen Corp.) was injected intravenously at 150 mg/kg 5 min before imaging. The mice were imaged using an IVIS 200 bioluminescence imaging system. Photons emitted from the luciferase-expressing cells within each tumor were measured in standardized regions of interest and quantified using the software program Living Images as an overlay on IGOR software (Wavemetrics, Portland, OR). A standardized rectangular region encompassing the head and neck of the mouse in a dorsal position was used to measure the bioluminescence signal. The animals were imaged on day 0 (time of inoculation) and twice a week thereafter.

2.7 Micro-PET/CT imaging

Tumor-bearing mice (n = 3) were treated with an intratumoral (IT) injection of PEG[^{64}Cu]CuS NPs (2 mM CuS molecules, 20 μL, 7.4 MBq/mouse). Twenty-four hours after injection of the radiolabeled NPs, the mice were anesthetized with 2% isoflurane and placed in the prone position, and micro-PET/CT images were acquired using an Inveon micro-PET/CT scanner (Siemens Preclinical Solution, Knoxville, TN). At the end of the imaging session (48 h after NPs injection), the mice were euthanized by CO_2 overexposure.

2.8 Biodistribution and dosimetry

Groups of tumor-bearing mice (n = 5 or 6/group) received IT or intravenous (IV) injections of PEG-[^{64}Cu]CuS NPs (2 mM CuS molecules, 200 μL, 7.4 MBq/mouse). At 0.25, 1, 2, 4, and 24 h after NP injection, mice were killed; blood, heart, liver, spleen, kidney, lung, stomach, intestine, muscle, bone, brain, and tumor tissues were removed and weighed; and radioactivity was measured with a Packard Cobra gamma counter (Ramsey, MN). Uptake of PEG-[^{64}Cu]CuS NPs in various organs was expressed as a percentage of the injected dose per gram of tissue (%ID/g).

For dosimetry, the means of organ and tumor %ID/g values at each time point were divided by 100 to convert to fraction of injected dose per gram of tissue (FID/g). The FID/g-versus-time data for each organ and tumor were then fit to either a single exponential or sum of two exponentials function, and the area under the fitted exponential curve was integrated from time = 0 to ∞, to compute residence time τ (normalized cumulative activity, MBq-h/MBq) per gram. Mouse organ τ per gram values were extrapolated to reference adult human residence times τ by multiplying by a mouse-to-reference adult human mass (M) correction

factor, $M_{TotalBodyMouse} \times (M_{OrganHuman}/M_{TotalBodyHuman})$, to account for differences in relative perfusion of organs between mice and humans [27]. Reference adult human normalized organ dose estimates (mGy/MBq) for both IT and IV injection of PEG-[^{64}Cu]CuS NPs were calculated using the internal radionuclide dosimetry program OLINDA/EXM 1.1 [27] and the extrapolated organ residence times.

The tumor residence time for each injection route (IT or IV) was computed by multiplying the tumor τ per gram value by the mean tumor mass for each corresponding group of mice. The estimated normalized tumor dose (mGy/MBq) for each group was then derived from the OLINDA/EXM 1.1 unit density sphere model self-dose factor table for ^{64}Cu (mGy/MBq-h) via multiplication by the residence time.

2.9 Determination of optimal laser power for treatment

Hth83 tumors in nude mice were treated with a 980-nm laser at power densities of 1, 2, 2.5, and 3 W/cm^2. The tissues were removed 24 h after treatment, snap frozen, and sliced into 6-μm section. Apoptosis was measured with a terminal deoxynucleotidyl transferase-mediated dUTP nick-end labeling kit (TUNEL kit; Promega Corporation, Madison, WI) according to the manufacturer's protocol, as previously described [28]. Briefly, slides were washed with phosphate-buffered saline and counterstained with DAPI. Immunofluorescence microscopy was carried out using a DMLA microscope (Leica Microsystems, Buffalo Grove, IL). Three slides from each group were selected, and apoptotic cells were quantified as the mean ratio of apoptotic cells to total cells in a 0.04-mm^2 field of each slide (200× magnification).

2.10 Antitumor activity

Twelve days after tumor cell inoculation, mice with Hth83-lucif tumors were randomized into 6 groups (n = 7 mice/group) with equivalent mean bioluminescence values. Mice in the control groups were not treated, were treated with laser alone, or were treated with PEG-CuS NPs alone (20 μL, optical density [OD] = 8). Mice in the RT group underwent IT injection of 20 μL of PEG-[^{64}Cu]CuS NPs (OD8; 400 μg/mL CuS NPs or ~0.1 μM CuS NPs; 7.4 MBq/mouse). Mice in the PTT group underwent IT injection of nonradioactive PEG-CuS NPs (20 μL, OD8) followed by NIR laser irradiation. Mice in the combined RT/PTT group underwent IT injection of PEG-[^{64}Cu]CuS NPs (20 μL, OD8, 7.4 MBq/mouse) followed by NIR laser irradiation. NIR laser light (980 nm) was delivered 24 h after NP injection at a power density of 2.5 W cm^{-2} for 2 min. After treatment, tumors were measured twice a week using an IVIS 200 bioluminescence imaging system to monitor tumor growth. Mice were euthanized if they lost more than 20% of their body weight or became moribund. Mouse body weight was measured twice a week to assess systemic toxicity. Survival curves were generated using GraphPad Prism software, version 6.01 (LaJolla, CA).

2.11 Statistical analysis

Quantitative data were expressed as mean ± SD. Means were compared using Student's *t* test. To determine significance of differences, a log-rank test was used. A p value of 0.05 or less was considered to be statistically significance.

3. Results

3.1 Nanoparticle synthesis and characterization

As shown in Figure 1A, PEG-[^{64}Cu]CuS NPs were synthesized by simply introducing Na_2S into an aqueous solution of $^{64}CuCl_2$ and $CuCl_2$ in the presence of PEG-SH. The radiochemical purity of PEG-[^{64}Cu]CuS NPs was 97.3% without purification (Supplementary Fig. S1). The representative TEM image of the PEG-CuS NPs revealed that the NPs were well dispersed with a mean diameter of 11.9 nm (Fig. 1B). In contrast, the mean hydrodynamic diameter of the PEG-[^{64}Cu]CuS NPs determined using dynamic light-scattering analysis was 29.8 nm (Supplementary Fig. S2). This result is attributable to the hydrophilic PEG coating on the CuS surface. The optical spectrum of the PEG-CuS NPs is shown in Figure 1C; the NPs had a strong absorption band in the NIR region (peak at ~ 930 nm). This feature of PEG-CuS NPs is an indication of their NIR light-induced thermal effect, which could be used for PTT.

Next, we investigated temperature elevation induced by NIR light irradiation in the presence of PEG-CuS NPs using a continuous-wave fiber-coupled diode laser centered at 980 nm. Figure 1D shows the temperature change of an aqueous solution of PEG-CuS NPs as a function of exposure time. Exposure to the NIR laser light at 2.5 W/cm^2 elevated the temperature of CuS NP solution (OD8, 400 μg/mL CuS NPs, ~0.1 μM CuS NPs) from 23°C to 98°C over a period of 10 min. The temperature of pure water was elevated only from 23°C to 32°C during the same per iod.

3.2 micro-PET/CT imaging

A micro-PET/CT imaging study was carried out to investigate the tissue retention of PEG-[^{64}Cu]CuS NPs after IT injection. The presence of tumor in the thyroid of the mice was confirmed by bioluminescence imaging (Fig. 2A). As shown in Figure 2B, most of the injected dose was retained in the tumor over a period of 48 h after IT injection of PEG-[^{64}Cu]CuS NPs. Quantitative analysis of the imaging data confirmed tumor retention of NPs (Fig. 2C). At 48 h after injection of PEG-[^{64}Cu]CuS NPs, about 50% of total injected dose remained at the tumor site, corresponding to a %ID/g value of 799 ± 107 %ID/g and a mean tumor weight of 61 mg. Radioactivity washed out from the tumor was primarily taken up by the liver (Fig. 2C).

3.3 Dosimetry after IV and IT injection

To assess whether PEG-[^{64}Cu]CuS NPs are suitable for radiotherapeutic applications, the organ distributions of PEG-[^{64}Cu]CuS NPs administered by IV and IT injection at various time points were obtained. As shown in Figure 3, the major organs having high uptakes of PEG-[^{64}Cu]CuS NPs after IV injection were the liver and the spleen. Uptake of the NPs in tumor gradually increased to ~6% ID/g at 24 h postinjection. In contrast, after IT injection, the concentration of PEG-[^{64}Cu]CuS NPs in tumor was initially extremely high (998% ID/g at 0.25 h postinjection) and decreased to 911% ID/g by 24 h postinjection and 799% by 48 h postinjection. In agreement with the imaging findings (Fig. 2B and 2C), NPs washed out from the tumors were redistributed to the liver and the spleen; the uptake of the NPs in the liver and the spleen increased from 1.78% ID/g and 3.0% ID/g, respectively, at 0.25 h

postinjection to 28.6% ID/g and 4.2% ID/g, respectively, at 24 h postinjection. These data suggest that a small fraction of the NPs injected into the tumor were gradually washed out from the injection site and captured by the organs of the reticuloendothelial system.

The estimated human radiation doses extrapolated from the mouse biodistribution data for PEG-[^{64}Cu]CuS NPs are presented in Table 1, while the integrated organ residence times from these data are presented in Table 2. These doses represent the normal dose per unit of injected activity delivered to the normal organs in an adult human. These data indicate that tumors are the primary critical organs. The tumor-absorbed doses were calculated to be 64.4 mGy/MBq for IV injection and 10,600 mGy/MBq for IT injection. In other words, the tumor-absorbed dose for IT injection was 165 times the tumor-absorbed dose for IV injection. Also, the residence time of PEG[^{64}Cu]CuS NPs in tumor with IT injection was 8.68 h, which was 140 times the residence time of the NPs in tumor with IV injection (only 0.062 h). The secondary critical organs were the heart wall (absorbed dose, 0.0155 mGy/MBq) for IT injection and the liver (absorbed dose, 0.099 mGy/MBq) for IV injection. The results of these calculations indicated that IT injection is a much better route than IV injection for local therapy for Hth83 ATC using PEG-[^{64}Cu]CuS NPs.

3.4 Optimization of laser power

To optimize tumor PTT, we tested the impact of laser power on normal thyroid tissue tolerance in mice. Figure 4A shows the mean ratio of apoptotic cells to live cells in normal thyroid tissues treated at laser power densities of 1, 2, 2.5, and 3 W/cm^2 for 2 min. When the laser power density reached 3 W/cm^2, the ratio of apoptotic cells to live cells was 47.0%, implying that almost half of treated cells died at this power. However, when the laser power density was 2.5 W/cm^2, the ratio was reduced to 12.2% (Fig. 4B). Therefore, 2.5 W/cm^2 was chosen for thyroid tumor treatment in the subsequent *in vivo* PTT studies.

3.5 Impact of RT/PTT on growth of ATC xenografts

To test the ability of PEG-[^{64}Cu]CuS NP-mediated RT/PTT to inhibit growth of ATC *in vivo*, we generated orthotopic ATC xenografts using cell lines expressing the luciferase gene. This allowed us to measure bioluminescence activity as a surrogate for tumor growth. Orthotopic thyroid tumors are not palpable until they grossly compress vital structures. By measuring the bioluminescence activity within each mouse tumor, we were able to identify the presence of tumor at an earlier stage and more accurately randomize the mice into treatment groups with similar tumor burden. Once treatment started, we quantified bioluminescence twice a week. This allowed us to follow tumor growth without having to rely on the less reliable external caliper method of measuring these highly infiltrative tumors that are deeply embedded in the thyroid gland and surrounding structures.

The mice with xenografts generated from Hth83-lucif cells were treated with nonradioactive PEG-CuS NPs at an injected dose of 20 μL (OD8, ~0.1 μM CuS NPs) or radioactive PEG-[^{64}Cu]CuS NPs at an injected dose of 20 μL (OD8, ~0.1 μM CuS NPs, 7.4 MBq/mouse). Figure 5A shows the experimental design for studying the *in vivo* anticancer effects of treatments with PEG-CuS NPs. Figures 5B and 5C show tumor growth curves and corresponding bioluminescence images for the six treatment groups (n = 7 mice/group).

Compared with no treatment, treatment with PEG-[^{64}Cu]CuS NPs plus NIR laser (combined RT/PTT) inhibited ATC tumor growth by 83.14% ($p = 0.032$). Similar tumor growth inhibition was observed for treatment with PEG-[^{64}Cu]CuS NPs alone (RT; 74.96% inhibition; $p = 0.036$), and treatment with PEG-CuS NPs plus NIR laser (PTT; 50.87% inhibition; $p = 0.078$). RT/PTT was significantly better in delaying tumor growth than PTT ($p = 0.026$). However, there was no significant difference in tumor growth inhibition between RT/PTT and RT ($p = 0.60$).

Survival probability was another metric used to evaluate the therapeutic effects of PEG-[^{64}Cu]CuS NPs. Figure 6A shows Kaplan–Meier survival curves following treatments with RT, PTT, and RT/PTT in the orthotopic Hth83 ATC model. Tumors progressed rapidly in the no-treatment control group (median survival time, 29 days), CuS NPs-alone group (30 days), and laser-alone group (28 days). Analysis with a log-rank test revealed that combined RT/PTT significantly prolonged the median survival time of tumor-bearing mice to 44 days ($p = 0.0022$) compared to survival in all three control groups (no treatment, laser alone, and NPs alone). RT and PTT also significantly prolonged the median survival time compared to survival in the control groups; median survival time with RT was 36 days ($p = 0.0053$), and median survival time with PTT was 35.5 days ($p = 0.069$). RT/PTT (median survival time, 44 days) resulted in better survival outcomes than PTT ($p = 0.067$). There was no difference in survival between RT/PTT and RT ($p = 0.25$). These findings indicated that the inhibition of tumor growth in mice treated with RT/PTT translated into an improved survival advantage.

3.6 Toxicity of treatment

Total body weight and general well-being of the mice were used as measures of toxicity. We did not notice any obvious signs of toxic effects in the PEG-CuS NPs-injected mice within 30 days after injection. Neither mortality nor noticeable reduction in body weight was observed in the control or treatment groups (Fig. 6B).

4. Discussion

ATC is one of the most lethal human cancers. In this study, we evaluated RT, PTT, and combined RT/PTT for the treatment of ATC in an orthotopic tumor model. Both RT and PTT were mediated through a single-compartment NP platform, PEG-[^{64}Cu]CuS NPs. We demonstrated that all three therapies were effective in delaying the growth of orthotopic ATC in nude mice and that combined RT/PTT was most effective in prolonging median survival. This single-compartment NP platform may represent a novel therapeutic option for ATC.

RT using ^{64}Cu has previously been described in a report of treatment with hypoxia-selective ^{64}Cu-diacetyl-bis(N4-methylthiosemicarbazone) (^{64}Cu-ATSM). These studies showed that ^{64}Cu-ATSM was effective in treating colorectal carcinoma in an *in vivo* tumor model [22]. *In vitro* studies demonstrated that ^{64}Cu-ATSM was taken up by tumor cells under hypoxic conditions and induced direct damage to DNA [29]. During decay, ^{64}Cu emits a 0.58-MeV β^- particle (40%), a 0.66-MeV β^+ particle (19%), and an electron capture delay with its associated Auger emissions (1.34 MeV, 41%). Auger electrons, because of

their short range (0.02–10 μm) and relatively larger linear energy transfer, are potentially more radiotoxic than the higher-energy β^- particles if localized in the nucleus [30]. The tissue penetration range of β^- particles emitted from ^{64}Cu is up to several hundred micrometers [29]. This is probably more important than the other decay modes for PEG-[^{64}Cu]CuS NPs delivered by IT injection because the NPs could have cytotoxic effects on both cells that took up the NPs and cells that did not take up the NPs. The cell-killing efficacy of ^{64}Cu is comparable to that of ^{67}Cu, another beta emitting copper radionuclide (0.6 MeV) [31]. When ^{67}Cu becomes more widely available, it will be worthwhile to also evaluate the radiotherapeutic effect of [^{67}Cu]PEG-CuS NPs because of their higher percentage of β^- decay (100%) and longer physical half-life ($t_{1/2}$ = 62 h) that may better match the longer retention of PEG-CuS NPs delivered by IT injection in the tumor.

^{64}Cu also emits β^+ radiation, allowing for the use of this radionuclide for PET and radiation dose estimation [20–24]. In fact, ^{64}Cu has been used to label various nanostructures, including gold NPs, quantum dots, carbon nanotubes, and polymeric NPs, for *in vivo* PET imaging of NPs' tissue distribution and tumor uptake [11, 25, 32–37]. In the present study, micro-PET imaging showed that radioactivity was largely retained in the tumor up to 48 h after IT injection (Fig. 2). The human absorbed dose was calculated on the basis of mouse biodistribution data. The maximal uptake of PEG-[^{64}Cu]CuS NPs in Hth83 tumor after IV injection was found to be 5.86 ± 0.99% ID/g at 24 h (Fig. 3A). The estimated radiation dose delivered to the Hth83 tumor was 64.4 mGy/MBq (Table 1). These values were higher than previously reported values for the tumor uptake of ^{64}Cu-ATSM (2.71% ID/g at 4 h postinjection) and the radiation dose delivered to GW39 colorectal tumor estimated on the basis of both biodistribution and PET imaging of ^{64}Cu-ATSM (15.4–21.9 MGy/MBq). Significant *in vivo* antitumor activity against GW39 tumor was demonstrated when ^{64}Cu-ATSM was injected at an IV dose of 370 MBq [22]. In the current study, since the estimated therapeutic dose delivered to the Hth83 tumor with IT injection was 165 times that delivered with IV injection, we focused our efforts on the antitumor activity of PEG-[^{64}Cu]CuS NPs delivered by IT injection. Our data confirmed that at an injected dose of only 7.4 MBq PEG-[^{64}Cu]CuS NPs alone displayed significant antitumor activity against Hth83 tumor. This result suggests that PEG-[^{64}Cu]CuS NPs were radiotoxic against Hth83 tumors.

Our findings indicate that combined RT/PTT mediated by IT injected PEG-[^{64}Cu]-CuS NPs resulted in enhanced antitumor activity compared to PTT alone. Significantly, this higher antitumor activity was achieved without causing apparent systemic toxic effects, as indicated by minimal changes in body weight for the mice in all treatment groups. Although further studies are needed to document both the acute and chronic toxicological effects of PEG-[^{64}Cu]CuS NPs after IT injection, PEG-[^{64}Cu]CuS NPs did exhibit several properties that make them a promising candidate for minimally invasive therapy for ATC. First, strong absorbance in the NIR region indicates that PEG[^{64}Cu]CuS NPs have high thermal conversion efficiency. In other words, injection of fewer PEG-[^{64}Cu]CuS NPs than the currently used OD8 solution should be possible. Second, the incorporation of ^{64}Cu into CuS NPs permits PET imaging and quantification of the NPs' retention in the tumor. This feature should aid future radiation dosimetry if this treatment is translated to the clinic. Third,

radiation decay from ^{64}Cu in PEG[^{64}Cu]CuS NPs is sufficient to cause substantial damage to the target cells with no acute systemic toxic effects.

Previous work has demonstrated that hyperthermia, a therapeutic procedure used to raise the temperature of tumor tissue, can potentiate RT [38, 39]. This potentiation of RT has been shown to be due to re-oxygenation of hypoxic tumor tissues after heating [40]. More recent work suggests that non-discriminating effect of hyperthermia on both cancer cells and cancer stem cells may be a mechanism for the radiosensitizing effect of heat [41]. Clearly, more studies are required to further elucidate the mechanism(s) of action for enhanced cell killing effect of combined RT/PTT mediated by PEG-[^{64}Cu]CuS NPs. In addition, further studies are warranted to investigate the effect of dose and dose schedule with combined RT/PTT mediated by PEG-[64Cu]CuS NPs.

Patients with ATC currently face a dismal prognosis with a median survival time of approximately 5 months. Aggressive locoregional disease invades normal neck structure causing vascular catastrophe and airway collapse. Surgery and radiation therapy are the only treatment modalities that can actually eradicate this disease. Chemotherapy may act as a radiosensitizer for radiotherapy or as a palliative treatment option. Novel therapeutic options such as intratumoral treatment with combined RT/PTT mediated by PEG-[^{64}Cu]CuS NPs are needed to address locoregional disease progression in order to prolong survival and improve quality of life.

5. Conclusion

In this study, we showed that tumor growth in mice bearing orthotopic Hth83 ATC tumors was inhibited by combined RT/PTT mediated by PEG-[^{64}Cu]CuS NPs compared to RT or PTT alone. Moreover, combined RT/PTT significantly prolonged the survival of orthotopic ATC tumor-bearing mice. In addition, tissue distribution of PEG-[^{64}Cu]CuS NPs could be imaged and quantified by PET, allowing dosimetry calculation and potential for prediction of thermal dose. Our data support the use of a single-compartment multifunctional NP system that acts as both a beta-emitter for effective RT and an efficient photothermal conducting agent for PTT. The combination of strong NIR absorption and integration of ^{64}Cu as a structural component makes these PEG[^{64}Cu]CuS NPs ideally suited for combined RT/PTT. Such an approach may represent a more effective means to treat ATC.

Supplementary Material

Refer to Web version on PubMed Central for supplementary material.

Acknowledgments

We thank Stephanie Deming for editing the manuscript. This work was supported in part by grants from the National Institutes of Health (U54CA151668) and the John S. Dunn Foundation and by Cancer Center Support Grant P30CA016672, which supports MD Anderson’s Small Animal Imaging Facility and High Resolution Electron Microscopy Facility.

References

1. Siegel R, Naishadham D, Jemal A. Cancer statistics, 2013. Ca-Cancer J Clin. 2013; 63:11–30. [PubMed: 23335087]
2. Chen AY, Jemal A, Ward EM. Increasing incidence of differentiated thyroid cancer in the united states, 1988–2005. Cancer. 2009; 115:3801–7. [PubMed: 19598221]
3. Society AC. Cancer Facts & Figures 2010. American Cancer Society; Atlanta, GA: 2010.
4. Smallridge RC, Copland JA. Anaplastic thyroid carcinoma: Pathogenesis and emerging therapies. Clin Oncol (R Coll Radiol). 2010; 22:486–97. [PubMed: 20418080]
5. McIver B, Hay ID, Giuffrida DF, Dvorak CE, Grant CS, Thompson GB, et al. Anaplastic thyroid carcinoma: A 50-year experience at a single institution. Surgery. 2001; 130:1028–34. [PubMed: 11742333]
6. Bhatia A, Rao A, Ang KK, Garden AS, Morrison WH, Rosenthal DI, et al. Anaplastic thyroid cancer: Clinical outcomes with conformal radiotherapy. Head Neck. 2010; 32:829–36. [PubMed: 19885924]
7. Sherman EJ, Lim SH, Ho AL, Ghossein RA, Fury MG, Shaha AR, et al. Concurrent doxorubicin and radiotherapy for anaplastic thyroid cancer: A critical re-evaluation including uniform pathologic review. Radiother Oncol. 2011; 101:425–30. [PubMed: 21981877]
8. Gule MK, Chen YY, Sano D, Frederick MJ, Zhou G, Zhao M, et al. Targeted therapy of VEGFR2 and EGFR significantly inhibits growth of anaplastic thyroid cancer in an orthotopic murine model. Clin Cancer Res. 2011; 17:2281–91. [PubMed: 21220477]
9. Isham CR, Bossou AR, Negron V, Fisher KE, Kumar R, Marlow L, et al. Pazopanib enhances paclitaxel-induced mitotic catastrophe in anaplastic thyroid cancer. Sci Transl Med. 2013; 5
10. Melancon MP, Zhou M, Li C. Cancer theranostics with near-infrared light-activatable multimodal nanoparticles. Acc Chem Res. 2011; 44:947–56. [PubMed: 21848277]
11. Lu W, Xiong C, Zhang G, Huang Q, Zhang R, Zhang JZ, et al. Targeted photothermal ablation of murine melanomas with melanocyte-stimulating hormone analog-conjugated hollow gold nanospheres. Clin Cancer Res. 2009; 15:876–86. [PubMed: 19188158]
12. Melancon MP, Lu W, Yang Z, Zhang R, Cheng Z, Elliot AM, et al. In vitro and in vivo targeting of hollow gold nanoshells directed at epidermal growth factor receptor for photothermal ablation therapy. Mol Cancer Ther. 2008; 7:1730–9. [PubMed: 18566244]
13. Melancon MP, Elliott A, Ji X, Shetty A, Yang Z, Tian M, et al. Theranostics with multifunctional magnetic gold nanoshells: Photothermal therapy and T2* magnetic resonance imaging. Invest Radiol. 2011; 46:132–40. [PubMed: 21150791]
14. Zhou M, Zhang R, Huang M, Lu W, Song S, Melancon MP, et al. A chelator-free multifunctional [^{64}Cu]CuS nanoparticle platform for simultaneous micro-PET/CT imaging and photothermal ablation therapy. J Am Chem Soc. 2010; 132:15351–8. [PubMed: 20942456]
15. Song SL, Xiong CY, Zhou M, Lu W, Huang Q, Ku G, et al. Small-animal PET of tumor damage induced by photothermal ablation with (64)Cu-bis-dota-hypericin. J Nucl Med. 2011; 52:792–9. [PubMed: 21498539]
16. Ku G, Zhou M, Song SL, Huang Q, Hazle J, Li C. Copper sulfide nanoparticles as a new class of photoacoustic contrast agent for deep tissue imaging at 1064 nm. Acs Nano. 2012; 6:7489–96. [PubMed: 22812694]
17. Chang CH, Stabin MG, Chang YJ, Chen LC, Chen MH, Chang TJ, et al. Comparative dosimetric evaluation of nanotargeted (188)Re-(DXR)-liposome for internal radiotherapy. Cancer Biother Radiopharm. 2008; 23:749–58. [PubMed: 19111045]
18. Chanda N, Kan P, Watkinson LD, Shukla R, Zambre A, Carmack TL, et al. Radioactive gold nanoparticles in cancer therapy: Therapeutic efficacy studies of GA-198AuNP nanoconstruct in prostate tumor-bearing mice. Nanomedicine. 2010; 6:201–9. [PubMed: 19914401]
19. Hong H, Zhang Y, Sun J, Cai W. Molecular imaging and therapy of cancer with radiolabeled nanoparticles. Nano Today. 2009; 4:399–413. [PubMed: 20161038]
20. Anderson CJ, Ferdani R. Copper-64 radiopharmaceuticals for PET imaging of cancer: Advances in preclinical and clinical research. Cancer Biother Radiopharm. 2009; 24:379–93. [PubMed: 19694573]

21. Bryan JN, Jia F, Mohsin H, Sivaguru G, Anderson CJ, Miller WH, et al. Monoclonal antibodies for copper-64 PET dosimetry and radioimmunotherapy. Cancer Biol Ther. 2011; 11:1001–7. [PubMed: 21464612]
22. Lewis JS, Laforest R, Buettner TL, Song SK, Fujibayashi Y, Connett JM, et al. Copper-64-diacetyl-bis(N-4-methylthiosemicarbazone): An agent for radiotherapy. Proc Nat Acad Sci U S A. 2001; 98:1206–11.
23. Shokeen M, Anderson CJ. Molecular imaging of cancer with copper-64 radiopharmaceuticals and positron emission tomography (PET). Acc Chem Res. 2009; 42:832–41. [PubMed: 19530674]
24. Laforest R, Dehdashti F, Lewis JS, Schwarz SW. Dosimetry of 60/61/62/64Cu-ATSM: A hypoxia imaging agent for PET. Eur J Nucl Med Mol Imaging. 2005; 32:764–70. [PubMed: 15785955]
25. Rossin R, Pan D, Qi K, Turner JL, Sun X, Wooley KL, et al. ^{64}Cu-labeled folate-conjugated shell cross-linked nanoparticles for tumor imaging and radiotherapy: Synthesis, radiolabeling, and biologic evaluation. J Nucl Med. 2005; 46:1210–8. [PubMed: 16000291]
26. Zhao M, Sano D, Pickering CR, Jasser SA, Henderson YC, Clayman GL, et al. Assembly and initial characterization of a panel of 85 genomically validated cell lines from diverse head and neck tumor sites. Clin Cancer Res. 2011; 17:7248–64. [PubMed: 21868764]
27. Stabin MG, Sparks RB, Crowe E. Olinda/exm: The second-generation personal computer software for internal dose assessment in nuclear medicine. J Nuc Med. 2005; 46:1023–7.
28. Adachi M, Cui C, Dodge CT, Bhayani MK, Lai SY. Targeting Stat3 inhibits growth and enhances radiosensitivity in head and neck squamous cell carcinoma. Oral Oncol. 2012; 48:1220–6. [PubMed: 22770899]
29. Obata A, Kasamatsu S, Lewis JS, Furukawa T, Takamatsu S, Toyohara J, et al. Basic characterization of Cu-64-ATSM as a radiotherapy agent. Nucl Med Biol. 2005; 32:21–8. [PubMed: 15691658]
30. ODonoghue JA, Wheldon TE. Targeted radiotherapy using auger electron emitters. Phys Med Biol. 1996; 41:1973–92. [PubMed: 8912375]
31. Blower PJ, Lewis JS, Zweit J. Copper radionuclides and radiopharmaceuticals in nuclear medicine. Nucl Med Biol. 1996; 23:957–80. [PubMed: 9004284]
32. You J, Zhang R, Xiong C, Zhong M, Melancon M, Gupta S, et al. Effective photothermal chemotherapy using doxorubicin-loaded gold nanospheres that target EphB4 receptors in tumors. Cancer Res. 2012; 72:4777–86. [PubMed: 22865457]
33. Liu Z, Cai WB, He LN, Nakayama N, Chen K, Sun XM, et al. In vivo biodistribution and highly efficient tumour targeting of carbon nanotubes in mice. Nat Nanotechnol. 2007; 2:47–52. [PubMed: 18654207]
34. Pressly ED, Rossin R, Hagooly A, Fukukawa KI, Messmore BW, Welch MJ, et al. Structural effects on the biodistribution and positron emission tomography (PET) imaging of well-defined Cu-64-labeled nanoparticles comprised of amphiphilic block graft copolymers. Biomacromolecules. 2007; 8:3126–34. [PubMed: 17880180]
35. Schipper ML, Cheng Z, Lee SW, Bentolila LA, Iyer G, Rao JH, et al. MicroPET - based biodistribution of quantum dots in living mice. J Nucl Med. 2007; 48:1511–8. [PubMed: 17704240]
36. Schipper ML, Iyer G, Koh AL, Cheng Z, Ebenstein Y, Aharoni A, et al. Particle size, surface coating, and pegylation influence the biodistribution of quantum dots in living mice. Small. 2009; 5:126–34. [PubMed: 19051182]
37. Schluep T, Hwang J, Hildebrandt IJ, Czernin J, Choi CHJ, Alabi CA, et al. Pharmacokinetics and tumor dynamics of the nanoparticle IT-101 from PET imaging and tumor histological measurements. Proc Natl Acad Sci U S A. 2009; 106:11394–9. [PubMed: 19564622]
38. van der Zee J, Gonzalez DG, van Rhoon GC, van Dijk JDP, van Putten WLJ, Hart AAM, et al. Comparison of radiotherapy alone with radiotherapy plus hyperthermia in locally advanced pelvic tumours: A prospective, randomised, multicentre trial. Lancet. 2000; 355:1119–25. [PubMed: 10791373]
39. Horsman MR, Overgaard J. Hyperthermia: A potent enhancer of radiotherapy. Clin Oncol (R Coll Radiol). 2007; 19:418–26. [PubMed: 17493790]

40. Sun XR, Xing LG, Ling CC, Li GC. The effect of mild temperature hyperthermia on tumour hypoxia and blood perfusion: Relevance for radiotherapy, vascular targeting and imaging. Int J Hyperther. 2010; 26:224–31.

41. Tecchio C, Colato C, Bonifacio M, Krampera M, Maluta S, Pizzolo G, et al. Plasmacytoid dendritic cell leukemia: A rapidly evolving disease presenting with skin lesions sensitive to radiotherapy plus hyperthermia. Oncologist. 2009; 14:1205–8. [PubMed: 19939893]

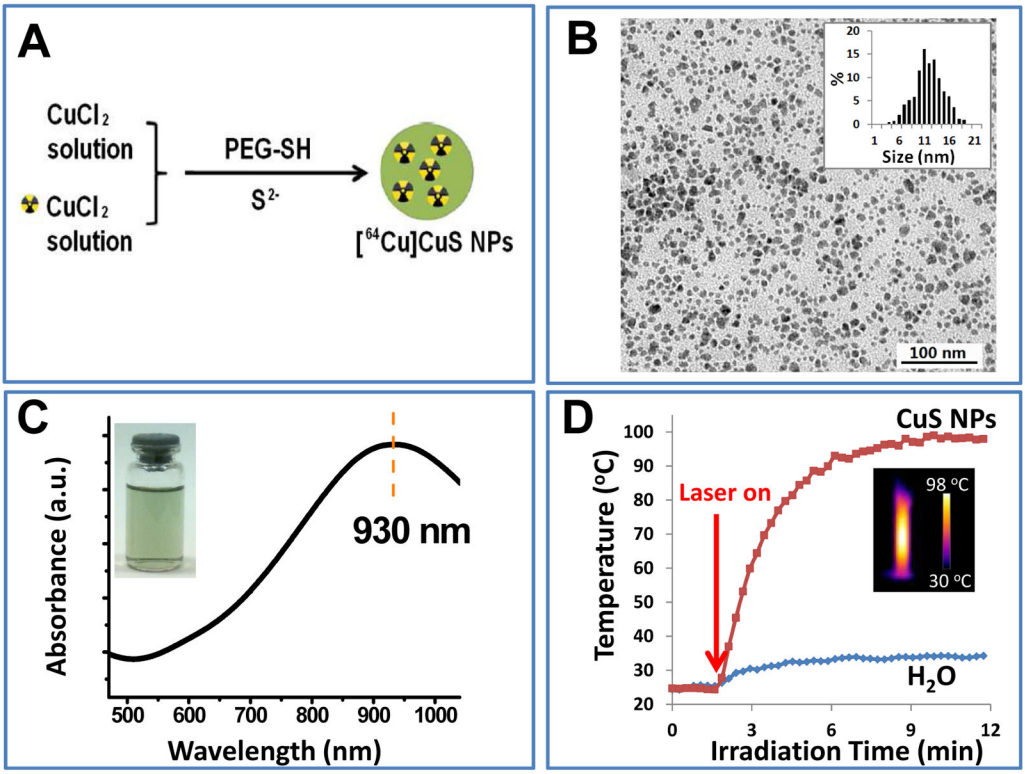

Figure 1.

Synthesis and characterization of PEG-CuS NPs. (A) Scheme for fabrication of PEG-[^{64}Cu]CuS NPs. (B) Transmission electron microscopic image of PEG-CuS NPs. Inset: particle size distribution. (C) Ultraviolet–visible spectrum of CuS NPs. Inset: photograph of an aqueous solution of CuS NPs after 6 months of storage at 4°C in the presence of argon. (D) Temperature ch ange curve of PEG-CuS NPs solution under 980 nm NIR laser irradiation. Pure water was used as a control. Inset: corresponding thermo-image of PEG-CuS NPs under laser irradiation at 10 min.

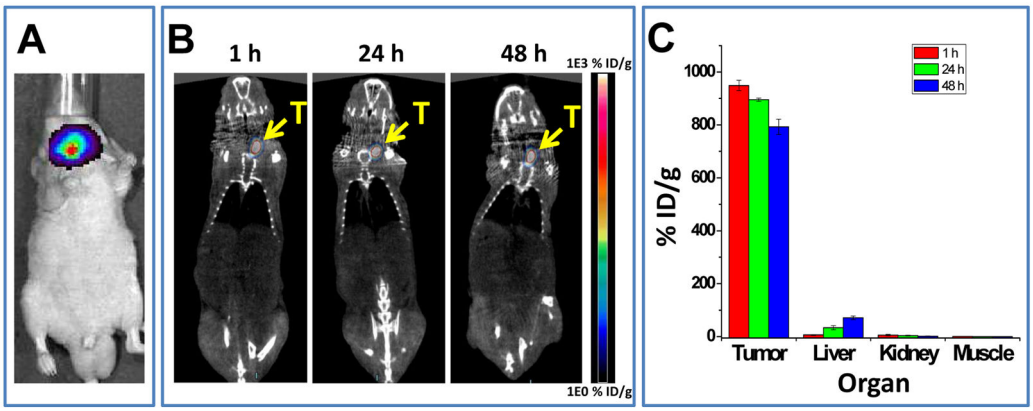

Figure 2.

(A) Representative superimposed photograph and bioluminescence image of Hth83 ATC tumor-bearing mouse. (B) Representative micro-PET/CT images and (C) graph of NP distribution in major organs of Hth83 ATC tumor-bearing mice at 1, 24, and 48 h after intratumoral injection of PEG-[^{64}Cu]CuS NPs.

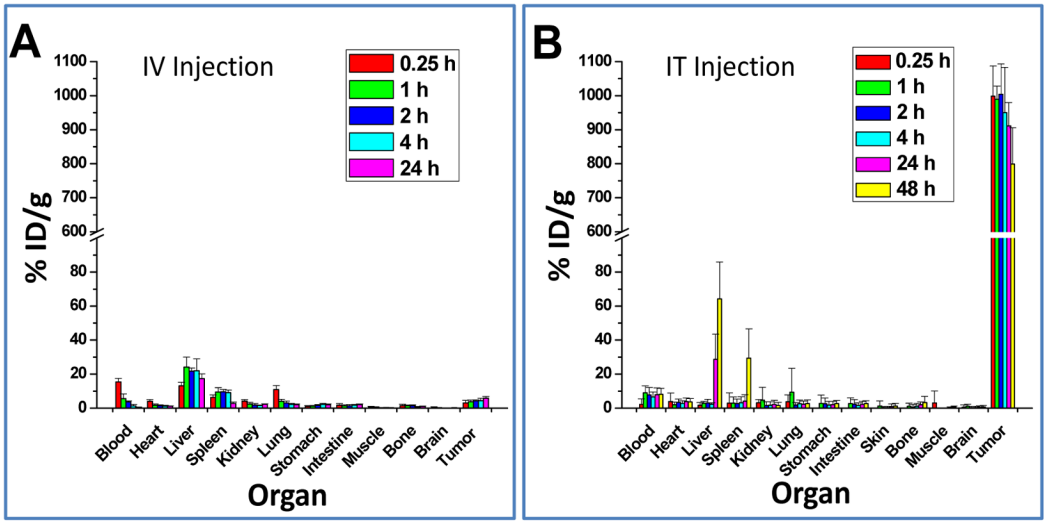

Figure 3.

Biodistribution of PEG-[^{64}Cu]CuS NPs in Hth83 ATC orthotopic mouse model. (A) Intravenous injection, and (B) intratumoral injection.

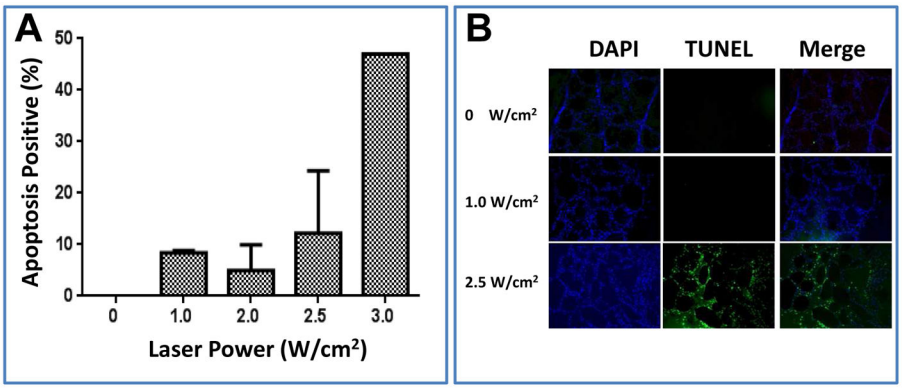

Figure 4.

Impact of laser power density on percentage of apoptosis in normal thyroid tissues in mice. (A) Percentage of cells positive for apoptosis. (B) TUNEL staining.

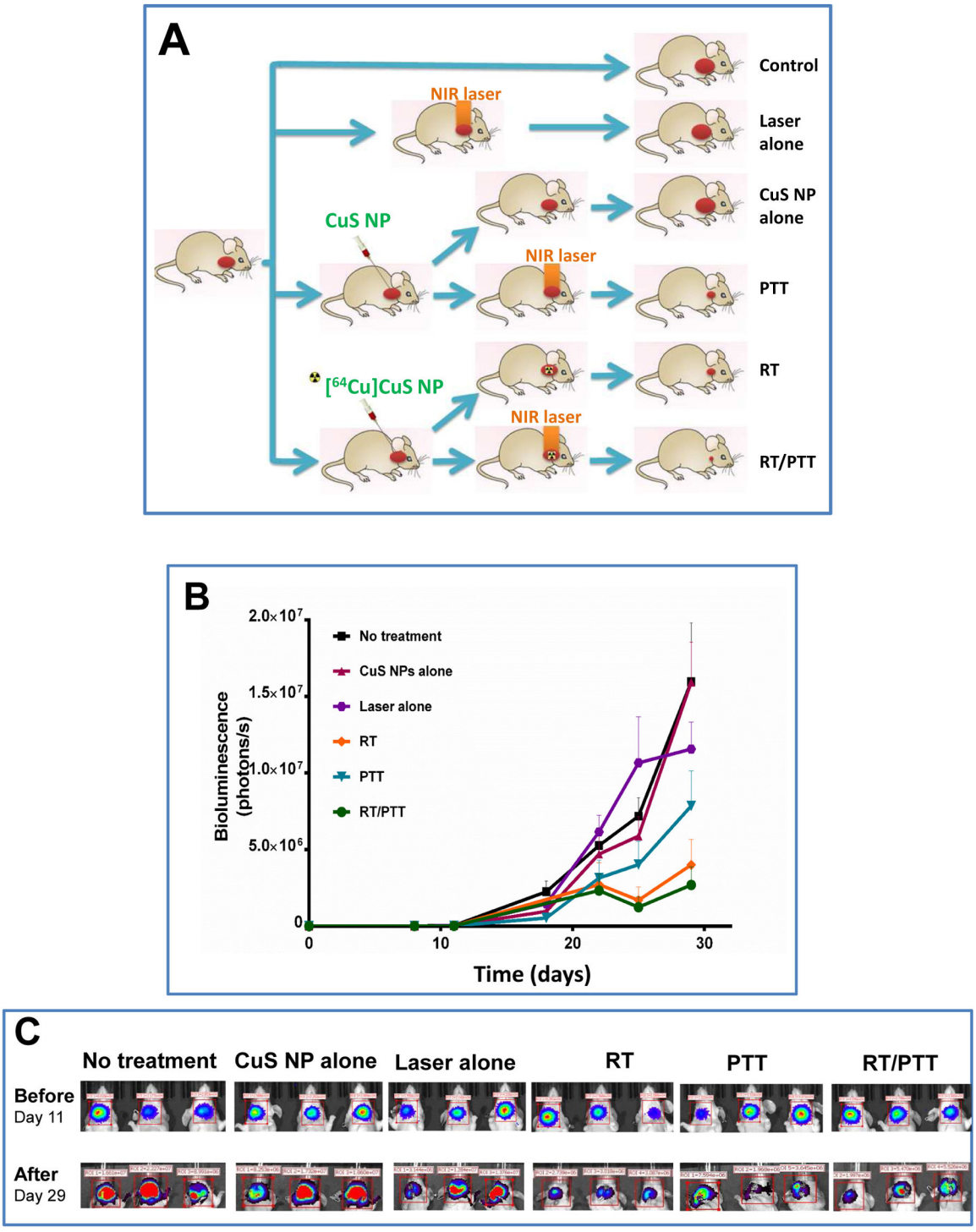

Figure 5.

(A) Experimental design of the antitumor activity study in nude mice bearing subcutaneous ATC tumors (n = 7/group). (B, C) Tumor growth curves and corresponding bioluminescence images after treatment with CuS NPs alone, laser alone, radiotherapy (RT), photothermal

therapy (PTT), or combined radio-photothermal therapy (RT/PTT). A group of mice without treatment was used as a control.

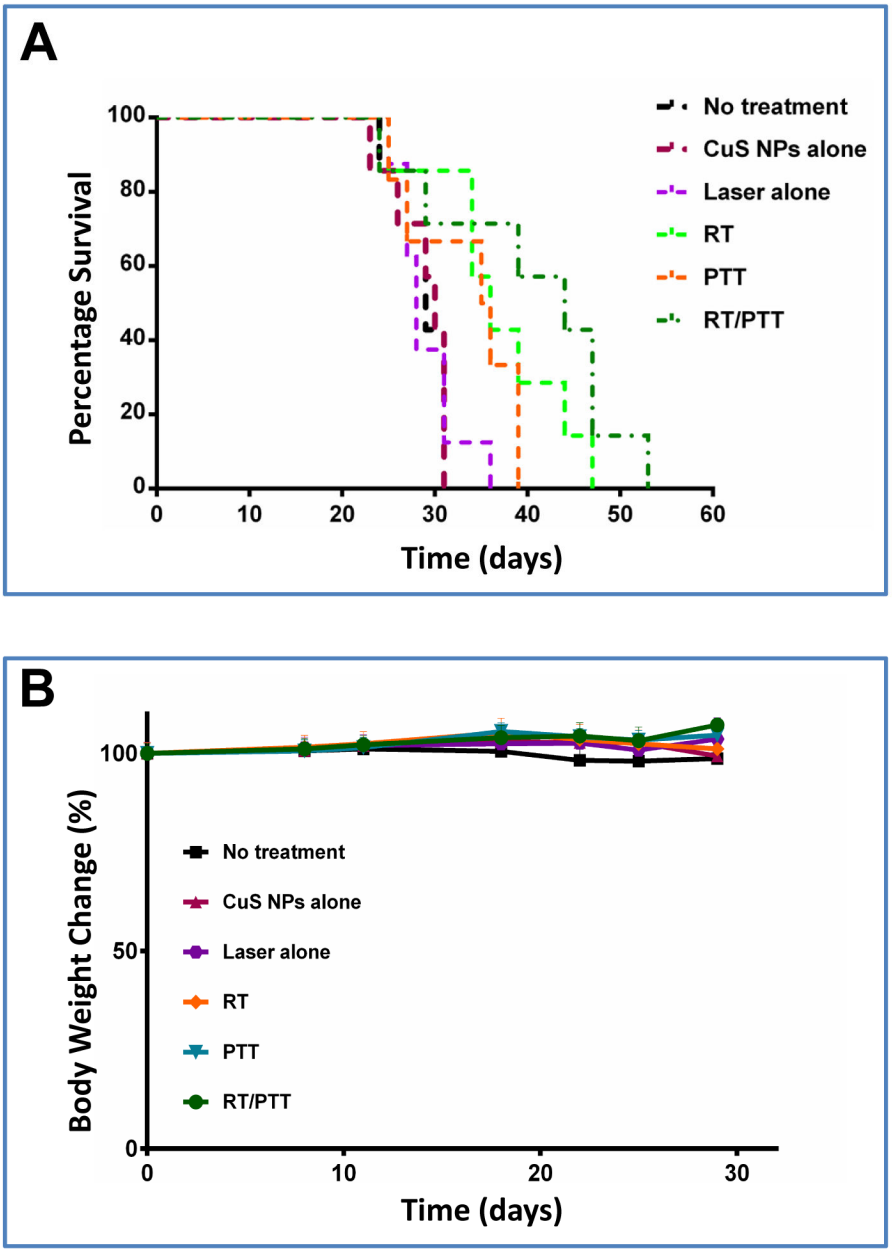

Figure 6.

(A) Kaplan–Meier survival curves of Hth83 ATC tumor-bearing mice after treatment with CuS NPs alone, laser alone, RT, PTT, or RT/PTT (n = 7/group). Mice without treatment were used as a control. (B) Body weight changes after treatment with CuS NPs alone, laser alone, RT, PTT, or RT/PTT. A group of mice without treatment was used as a control.

Table 1

Estimated human absorbed radiation doses extrapolated from mouse biodistribution data for PEG-[^{64}Cu]CuS NPs

Target Organ	Absorbed Dose (mGy/MBq), IT Injection	Absorbed Dose (mGy/MBq), IV Injection
Tumor	1.06×10^{4}	64.4
Adrenals	1.38×10^{-3}	5.23×10^{-3}
Brain	2.76×10^{-3}	1.20×10^{-3}
Breasts	5.15×10^{-4}	1.24×10^{-3}
Gallbladder wall	1.37×10^{-3}	9.06×10^{-3}
Lower large intestine wall	6.90×10^{-3}	6.48×10^{-3}
Small intestine	9.04×10^{-3}	9.44×10^{-3}
Stomach wall	3.78×10^{-3}	5.26×10^{-3}
Upper large intestine wall	6.22×10^{-3}	7.49×10^{-3}
Heart wall	1.55×10^{-2}	8.98×10^{-3}
Kidneys	6.39×10^{-3}	1.49×10^{-2}
Liver	6.55×10^{-3}	9.91×10^{-2}
Lungs	7.55×10^{-3}	1.32×10^{-2}
Muscle	1.81×10^{-3}	2.77×10^{-3}
Ovaries	1.25×10^{-3}	1.52×10^{-3}
Pancreas	1.42×10^{-3}	4.79×10^{-3}
Red marrow	1.06×10^{-2}	4.64×10^{-3}
Osteogenic cells	2.31×10^{-2}	8.13×10^{-3}
Skin	4.60×10^{-4}	7.88×10^{-4}
Spleen	2.02×10^{-2}	3.02×10^{-2}
Testes	4.12×10^{-4}	4.15×10^{-4}
Thymus	7.99×10^{-4}	1.30×10^{-3}
Thyroid	6.15×10^{-4}	64.4
Urinary bladder wall	6.28×10^{-4}	7.78×10^{-4}
Uterus	9.81×10^{-4}	1.25×10^{-3}
Total body	2.38×10^{-3}	5.04×10^{-3}
Effective Dose Eq. (mSv/MBq)	6.77×10^{-3}	1.27×10^{-2}
Effective Dose (mSv/MBq)	4.61×10^{-3}	9.42×10^{-3}

Table 2

Organ residence times of PEG-[^{64}Cu]CuS NPs estimated from mouse biodistribution data.

Source Organ	Residence Time (h), IT injection	Residence Time (h), IV injection
Tumor	8.68	0.062
Brain	0.036	0.015
Lower large intestine wall	0.022	0.021
Small intestine	0.090	0.083
Stomach wall	0.018	0.018
Upper large intestine wall	0.029	0.027
Heart wall	0.059	0.024
Kidneys	0.020	0.042
Liver	0.13	2.10
Lungs	0.088	0.14
Muscle	0.42	0.54
Red marrow	0.12	0.038
Cortical bone	0.21	0.064
Trabecular bone	0.34	0.10
Spleen	0.044	0.065